

# GOLF BALL AERODYNAMICS

A DISSERTATION SUBMITTED TO THE UNIVERSITY OF MANCHESTER  
FOR THE DEGREE OF MASTER OF SCIENCE  
IN THE FACULTY OF ENGINEERING AND PHYSICAL SCIENCES

2014

**James Fielder**  
School of Mathematics

# Contents

<b>Abstract</b>	<b>6</b>
<b>Declaration</b>	<b>7</b>
<b>Intellectual Property Statement</b>	<b>8</b>
<b>Acknowledgements</b>	<b>9</b>
<b>1 Introduction</b>	<b>10</b>
1.1 A Brief History of Golf . . . . .	10
1.2 A Slightly Larger History of the Golf Ball . . . . .	11
1.3 Aims of the Project . . . . .	12
<b>2 Preliminary Investigations and Background</b>	<b>13</b>
2.1 Projectile Motion . . . . .	13
2.1.1 3D Projectile Motion . . . . .	15
2.2 Basic Aerodynamics . . . . .	16
2.2.1 Fluid Mechanics . . . . .	16
2.2.2 Non Dimensional Variables and the Reynolds Number . . . . .	17
2.2.3 Boundary Layers . . . . .	19
2.2.4 Lift and Drag . . . . .	20
2.2.5 Boundary Layer Separation and the Magnus Effect . . . . .	22
2.2.6 The Drag Crisis . . . . .	23
2.3 Previous Work on Modelling Golf Ball Flight . . . . .	25
2.3.1 Computational Simulations of Golf Ball Flight . . . . .	27
2.4 Measuring Golf Ball Trajectories . . . . .	28

<b>3</b>	<b>A Model of Golf Ball Flight</b>	<b>30</b>
3.1	A Model for Golf Ball Flight . . . . .	30
3.1.1	Lift and Drag . . . . .	30
3.1.2	Accounting for the Wind . . . . .	32
3.1.3	The Equations of Motion . . . . .	32
3.1.4	An Example Trajectory . . . . .	33
3.2	Limitations of the Model . . . . .	35
3.2.1	Comparing Trajectories with Data . . . . .	36
3.3	Improvements . . . . .	39
<b>4</b>	<b>Improving <math>c_D</math></b>	<b>40</b>
4.1	Estimating $c_D$ from Experiments . . . . .	40
4.2	Parameterising $c_D$ and $c_L$ by Non Dimensional Variables . . . . .	43
4.3	tanh Matching . . . . .	44
<b>5</b>	<b>Conclusions</b>	<b>45</b>
5.1	Possible Future Work . . . . .	45
<b>A</b>	<b>Inverse Problems and Least Squares</b>	<b>46</b>
A.1	Inverse Problems . . . . .	46
A.2	Least Squares . . . . .	46
A.2.1	Guass-Newton Method . . . . .	46
A.2.2	Levenberg-Marquardt Algorithm . . . . .	46
A.2.3	Trust Region Method . . . . .	46
A.3	Well Posedness and Regularization . . . . .	46

# List of Tables

2.1 List of fundamental dimensions . . . . . 18

# List of Figures

1.1	Images of golf balls . . . . .	11
2.1	Diagram of the separation points in the Magnus Effect . . . . .	22
2.2	A diagram of the Magnus effect . . . . .	23
2.3	Plot of the Morrison drag formula . . . . .	24
3.1	2D plot of an example Robinson and Robinson model trajectory . . . .	34
3.2	3D plot of an example Robinson and Robinson model trajectory . . . .	34
3.3	Plotting the data against an example Robinson and Robinson trajectory	37
3.4	Plotting the data against an example Robinson and Robinson trajectory in 3D . . . . .	37
3.5	Plot of speed in Robinson and Robinson model against the speed in the data . . . . .	38
4.1	Plotting the original Morrison form against a modified version for golf balls . . . . .	41
4.2	Model with using the modified Morrison form for $c_D$ . . . . .	42
4.3	Model with using the modified Morrison form for $c_D$ in 3D. . . . .	43

# Abstract

In this project we work on golf balls and stuff.

# Declaration

No portion of the work referred to in the dissertation has been submitted in support of an application for another degree or qualification of this or any other university or other institute of learning.

# Intellectual Property Statement

- i. The author of this dissertation (including any appendices and/or schedules to this dissertation) owns certain copyright or related rights in it (the “Copyright”) and s/he has given The University of Manchester certain rights to use such Copyright, including for administrative purposes.
- ii. Copies of this dissertation, either in full or in extracts and whether in hard or electronic copy, may be made **only** in accordance with the Copyright, Designs and Patents Act 1988 (as amended) and regulations issued under it or, where appropriate, in accordance with licensing agreements which the University has entered into. This page must form part of any such copies made.
- iii. The ownership of certain Copyright, patents, designs, trade marks and other intellectual property (the “Intellectual Property”) and any reproductions of copyright works in the dissertation, for example graphs and tables (“Reproductions”), which may be described in this dissertation, may not be owned by the author and may be owned by third parties. Such Intellectual Property and Reproductions cannot and must not be made available for use without the prior written permission of the owner(s) of the relevant Intellectual Property and/or Reproductions.
- iv. Further information on the conditions under which disclosure, publication and commercialisation of this dissertation, the Copyright and any Intellectual Property and/or Reproductions described in it may take place is available in the University IP Policy (see <http://documents.manchester.ac.uk/DocuInfo.aspx?DocID=487>), in any relevant Dissertation restriction declarations deposited in the University Library, The University Library’s regulations (see <http://www.manchester.ac.uk/library/aboutus/regulations>) and in The University’s Guidance on Presentation of Dissertations.



# Acknowledgements

I would like to thank my supervisor Prof. Jitesh Gajjar for his guidance during the project without which I would have been completely lost. Additionally, I would like to thank The R&A for their sponsorship of the project and Dr Steve Otto for his guidance and assistance.

# Chapter 1

## Introduction

Stuff here about the project and aims and such.

### 1.1 A Brief History of Golf

The origins of the game of golf are difficult to trace, with suggestions that the game originated in either Scotland, France, the Netherlands, China, or even going back as far as the Roman Empire. Golf in its more modern incarnation however, is agreed to have originated in 15th century Scotland, where the first written records of the game are (somewhat humorously) related to King James II of Scotland banning the game in 1457 for fear of a decrease in archery practice in its favour.

From the 18th century onwards golf began to take form fully in Scotland, with the founding of both The Royal and Ancient Golf Club in St Andrews and The Royal Burgess Golfing Society in Edinburgh. The oldest surviving rules of golf also date from this time and these rules have been in a state of constant revision up to the modern day.

In the 19th century the popularity of golf vastly increased, seeing larger numbers of people knowing and playing the game, and the start of the first major tournaments. Additionally, the game spread out to encompass much of the British empire, to the United States and eventually to Japan, making golf into a global sport supported by a plethora of associated manufacturers, sponsors and organisations.

In the modern day, golf is potentially one of the largest sports on earth, with golf tournaments, golf manufacturing and related industries accounting for hundreds of

billions of pounds of economic activity. If successful on the golf tournament circuit, golf professionals can earn huge sums in prize money. With the players themselves and their sponsors having such a vested interest in success having a consistent and fair rule set is of paramount importance and this is dealt with jointly by The R&A in most of the world and the USGA (United States Golf Association) in the Americas.

## 1.2 A Slightly Larger History of the Golf Ball

Golf ball technology has advanced greatly since the advent of the game. Initially, hard wooden balls were used for playing, however these were soon replaced with featherie balls which are leather pouches stuffed with feathers and then painted white.

The next major innovation in the design of golf balls came in 1848, when the gutta-percha ball was invented. This is the first ball to use a rubbery substance as continues to this day, and was easier to make into a proper sphere, unlike the previous types of ball. It was around this time that it was discovered that abrasions to the surface of the ball would improve the aerodynamic properties of the ball, making it easier to control the flight of the ball and increasing the distance at which the game could be played. This would start a series of innovations that would lead to today's dimpled balls, which we will discuss later.



(a) “Featherie” balls



(b) Pro V1 ball

Figure 1.1: In 1.1a are “Featherie” golf balls, taken from [https://en.wikipedia.org/wiki/File:Featherie\\_golf\\_ball.JPG](https://en.wikipedia.org/wiki/File:Featherie_golf_ball.JPG), and in 1.1b is a modern style ball, namely the Titleist Pro V1 ball.

After this the golf ball once again changed form with the advent of using wrapped rubber thread to help the ball to bounce better. This was coupled with the first usage of a plastic covering, in order to protect the rubber inside the ball on impact with the club. This cover also persists to this day, although the inside of the ball has seen significant development.

The modern golf ball has changed significantly from old designs. The interior of the ball is now usually a 3 piece rubber composite, with different properties in each rubber to maximize the controllability of the ball during play. The exterior is a polyurethane cover (normally white but some are in other colours) with usually between 300 to 400 dimples (though these can go as low as 200 dimples, and beyond 600 in some cases). The properties of the ball are stipulated to be within certain ranges, as set by The R&A and USGA in the rules of golf. The weight of a ball must not be greater than 45.93g, the diameter no less than 42.67mm and the ball must be spherically symmetric.

### **1.3 Aims of the Project**

The aim of this project is to obtain a model for how golf balls fly based on simple physical principles. Given this model we then wish to categorise individual balls based on measurements of their flight, and use this categorisation to predict trajectories for the ball

Finally, using this model, we will attempt to use a limited set of flight data (between 20 and 30 m) to predict the full flight for the ball.

## Chapter 2

# Preliminary Investigations and Background

In order to devise a simple model for golf ball flight we first must understand some prerequisite physics for projectiles and fluid dynamics for the airflow over the ball. Understanding how the fluid flows over the surface of the ball is crucial to understanding the difference between the flight of a golf ball and that of a standard projectile. Quantifying this effect will be a large component of this project.

There has been significant work done previously in understanding the fluid dynamics around a golf ball and how a golf ball flies. We will attempt to review some of this literature in this chapter and summarise previous work on the topic.

First though, we must understand how normal projectiles fly without taking into account fluid dynamics effects.

### 2.1 Projectile Motion

A projectile is a body fired into the air by an initial impulse and then allowed to fall back to ground under the action of gravity alone. This is the most naive and simplistic model of golf ball flight, completely ignoring all aerodynamic effects, however we must understand it before building up to a more complex model.

Consider motion in a 2 dimensional plane, labelled by  $x$  along the horizontal and  $y$  along the vertical. A projectile is given an initial speed of the form  $\mathbf{V}_0 = (v_x, v_y)$ . We set the origin of the coordinate system to be the point at the start of the trajectory,

$(x_0, y_0) = (0, 0)$ . In this problem the acceleration on the projectile, after the initial impulse, is constant and of the form

$$a_x = 0, \quad a_y = -g \quad (2.1.1)$$

where  $g$  is the acceleration due to gravity. Since the acceleration is constant we can use the standard formulas for motion under constant acceleration to derive the dynamics of the projectile [Young and Freedman \(2008\)](#), which are

$$v = v_0 + at \quad (2.1.2a)$$

$$x = v_0 t + \frac{1}{2}at^2 \quad (2.1.2b)$$

$$v^2 = v_0^2 + 2ax \quad (2.1.2c)$$

$$x = \left( \frac{v_0 + v}{2} \right) t. \quad (2.1.2d)$$

Where  $v$  is the speed at a time  $t$ ,  $x$  is the distance from the origin of the coordinate system,  $a$  is the acceleration and  $v_0$  is the initial speed.

We will write the equations in component form along the axes. Let  $\mathbf{V}_0$  be the initial velocity. In component form these will be

$$v_{0x} = v_0 \cos \alpha$$

along the  $x$ -axis and

$$v_{0y} = v_0 \sin \alpha$$

where  $v_0 = |\mathbf{V}_0|$  and  $\alpha$  is the angle  $\mathbf{V}_0$  makes with the  $x$ -axis. Now using [\(2.1.1\)](#) and [\(2.1.2a\)](#) we may find

$$v_x = v_0 \cos \alpha \quad (2.1.3a)$$

and

$$v_y = v_0 \sin \alpha - gt. \quad (2.1.3b)$$

Now, using [\(2.1.2b\)](#) (or by integrating [\(2.1.3\)](#) with respect to  $t$ ), we can obtain the standard formulas for the  $x$  and  $y$  positions during the flight of the projectile:

$$x = (v_0 \cos \alpha)t \quad (2.1.4a)$$

and

$$y = (v_0 \sin \alpha)t - \frac{1}{2}gt^2. \quad (2.1.4b)$$

Eliminating  $t$  between these equations demonstrates that projectiles follow parabolic paths, giving

$$y = x \tan \alpha - \frac{g}{2v_0^2 \cos^2 \alpha} x^2 \quad (2.1.5)$$

for the path of the projectile.

Finally we may use these equations to find the maximum height, range and time of flight for a projectile. The maximum height is obtained when  $v_y = 0$  and solving (2.1.3b) with this condition gives

$$t_H = \frac{v_0 \sin \alpha}{g}. \quad (2.1.6)$$

The range is obtained by solving for  $y = 0$  in (2.1.4b) and selecting the non trivial root for  $t$  of

$$t_F = \frac{2v_0 \sin \alpha}{g} \quad (2.1.7)$$

where  $t_F$  is the time of flight for the projectile. Inserting this into (2.1.4a) gives

$$x = \frac{2v_0^2 \cos \alpha \sin \alpha}{g}$$

and recalling that  $\sin 2\alpha = 2 \cos \alpha \sin \alpha$  gives

$$x = \frac{v_0^2 \sin 2\alpha}{g} \quad (2.1.8)$$

for the range of the projectile.

### 2.1.1 3D Projectile Motion

Projectile motion in 3 dimensions works in exactly the same fashion as 2D projectile motion. Here we will take the  $z$ -axis to be the vertical and  $x$  and  $y$  axes to be labelling the surface. The only component of acceleration is along the  $z$ -axis, with

$$a_z = -g$$

as before. All other equations remain the same.

## 2.2 Basic Aerodynamics

Of course, the flight of a golf ball is inevitably affected by aerodynamics. As such we need to have some understanding of how aerodynamic effects will . In particular, we will need to understand how boundary layers form on and separate from the surface of the golf ball and how this effects the drag on the ball. First we will review some basic fluid mechanics.

### 2.2.1 Fluid Mechanics

In this project we will model the air flowing around the ball as being an incompressible fluid. This is an Eulerian description of fluid flow, viewing the fluid as though the ball is fixed in the centre of the coordinate system and the fluid moving around the ball [Ruban and Gajjar \(2014\)](#).

We will not concern ourselves with a full discussion of fluid mechanics from basic principles here, instead we will simply state some useful results predominantly following [Ruban and Gajjar \(2014\)](#) and [Sears \(2011\)](#).

Let  $\mathbf{V}$  be the fluid velocity, which is a function of the the position  $\mathbf{r}$  from the origin of the coordinate system and of time  $t$ . Let  $\rho$  be the density of the fluid and  $p$  the pressure. We define the material derivative to be (as a differential operator)

$$\frac{D}{Dt} = \frac{\partial}{\partial t} + (\mathbf{V} \cdot \nabla)$$

and represents the rate of change of some quantity within the fluid, while moving with a small element of the fluid flow. That is, in a description where the fluid moves relative to the coordinate system the material derivative measures the rate of change as seen by a moving fluid element.

At all points within the fluid the mass continuity equation must apply

$$\frac{D\rho}{Dt} + \rho \nabla \cdot \mathbf{V} = 0. \tag{2.2.1}$$

This equation encodes the condition that mass is conserved within a fluid without any sources or sinks. In an incompressible fluid, as we will be primarily conserved with in this project,  $\rho$  will not change with time, and as such  $D\rho/Dt = 0$ . As a consequence, both terms on the left hand side of (2.2.1) must be zero everywhere within the fluid,



and therefore the equation reduces to

$$\nabla \cdot \mathbf{V} = 0 \quad (2.2.2)$$

for an incompressible fluid.

The continuity equation gives one equation for the velocity components  $u, v, w$ <sup>1</sup> within a fluid. In order to specify the pressure and velocity everywhere we therefore require three more equations to determine the system. These three equations are supplied by considerations of energy and momentum conservation. Keeping all of these in mind, we may write a momentum equation in the form

$$\rho \frac{D\mathbf{V}}{Dt} = -\nabla p + \mu \nabla^2 \mathbf{V} + \mathbf{f} \quad (2.2.3)$$

where  $\mathbf{f}$  is body force per unit volume acting on the fluid (for example a gravitational force) and  $\mu$  is the viscosity of the fluid.

Equations (2.2.2) and (2.2.3) when taken together form the Navier-Stokes equations for the velocity and pressure fields within an incompressible fluid. It is well known that these equations are highly non-linear and exceedingly difficult to solve both analytically and numerically, except in special circumstances.

From solutions the Navier-Stokes equations emerges a number of fascinating effects within fluid dynamics. In this project, we are particularly interested in boundary layer effects and turbulence.

### 2.2.2 Non Dimensional Variables and the Reynolds Number

In physics we are often interested in understanding the behaviour of a system independent of a choice of units [Misic et al. \(2010\)](#). Instead, we wish to have a system of measurement which does not depend intrinsically on one set on units, but on more fundamental ideas such as length or mass. We desire this for two main reasons:

- Physical statements should not have any dependency on the units they are stated in. Non-dimensionalising the problem ensures that this is the case.

---

<sup>1</sup> The convention within fluid mechanics is that the  $x, y, z$  velocity components are called  $u, v, w$  respectively. That is

$$v_x = u, \quad v_y = v, \quad v_z = w.$$

- Using non-dimensional variables allow problems of different scales to be compared to each other on an equal footing. Often the points when the physical behaviour of the system changes will depend on some non-dimensional parameter, as we will see with turbulence later [Jensen \(2013\)](#).

Additionally, analysing the fundamental dimensions of a physical problem can yield information on the functional form of quantities within the model without having to use more advanced mathematical techniques to derive such results. By simply understanding the dependency on fundamental units we often can find interesting scaling laws for functions of interest.

The fundamental dimensions (only those which will be useful in this project) are as follows:

Dimension	Symbol
Length	$L$
Mass	$M$
Time	$T$

Table 2.1: List of fundamental dimensions we will require in this report.

Any quantities of interest can be written using these variables: for example, an area  $A$  would have the dimensions  $[A] = L^2$  and a velocity  $[V] = L/T$ .

Physical laws can, in general, be written as [Misic et al. \(2010\)](#)

$$q_0 = f(q_1, q_2, \dots, q_n) \quad (2.2.4)$$

where  $q_0$  is a physical quantity we are interested in obtaining,  $q_1, \dots, q_n$  are independent physical quantities and  $f$  is a functional relationship between them.

When analysing the dimensions of a problem we must ensure that the following conditions are satisfied

- Both sides of (2.2.4) must have the same fundamental dimensions.
- Any sum of  $q_i$  must have the same dimensions.
- Any function of  $q_i$  (say, exponential or trigonometric) must be dimensionless. This is as a direct result of the last condition and being able to expand these functions as a power series.

We will demonstrate this technique in section 2.2.4.

One of the aims of dimensional analysis is to find groupings of physical quantities which are dimensionless. These have useful properties of scale invariance which leads to natural parameterisations for physical problems.

Within fluid mechanics one such dimensionless grouping which manifests often is the Reynolds number, defined as

$$Re = \frac{\rho \mathbf{V} L}{\mu}. \quad (2.2.5)$$

For a sphere,  $\mathbf{V}$ ,  $\mu$  and  $\rho$  are defined as they have already been in this text, and the characteristic length  $L$  is defined to be the diameter of the sphere. This quantity represents the ratio of inertial forces to viscous ones, and we will make considerable use of it within the project. The Reynolds number, in some ways, can be considered to be a non dimensional analogue of the velocity, taking into account the intrinsic length scale of the problem under consideration.

### 2.2.3 Boundary Layers

One of the fundamental ideas within fluid mechanics is that of the no slip condition. The no slip condition specifies that when a fluid encounters a solid body it must, at the surface of the body, take the velocity and temperature of that body. This means that there will be a thin layer of fluid around the body where the velocity changes from that of the overall stream to match the velocity of the solid body: this layer is referred to as the boundary layer.

The equations which govern the flow within the boundary layer are a simplified version of the Navier-Stokes equations, taking into account the order of magnitude of the boundary layer compared to the size of the body. The derivation of these equations completed by scaling the Navier-Stokes based on the assumption that the boundary layer is much smaller than the body size [Anderson \(1985\)](#).

In 2D these equations look as follows:

$$\frac{\partial u}{\partial x} + \frac{\partial v}{\partial y} = 0 \quad (\text{Continuity equation}) \quad (2.2.6a)$$

$$u \frac{\partial u}{\partial x} + v \frac{\partial u}{\partial y} = -\frac{1}{\rho} \frac{\partial p}{\partial x} + \nu \frac{\partial^2 u}{\partial y^2} \quad (x \text{ momentum}) \quad (2.2.6b)$$

$$\frac{1}{\rho} \frac{\partial p}{\partial y} = 0 \quad (y \text{ momentum}) \quad (2.2.6c)$$

where  $\nu$  is the kinematic viscosity, defined as  $\nu = \mu/\rho$ .

Boundary layer theory has been hugely important in the development of aerodynamics, taking previously intractable problems and facilitating a better understanding of the fluid dynamics of bodies [Anderson \(1985\)](#). The affect of the boundary layer will be important in the modelling of golf balls, as we will see later.

## 2.2.4 Lift and Drag

In order to go beyond modelling golf ball flight as simply that of a projectile we must understand how the lift and drag forces affect the flight of the ball. We can use dimensional analysis arguments to obtain a functional form for these effects. Here we follow the analysis of [Jensen \(2013\)](#) in order to demonstrate the analysis for the drag force. The lift is found in a similar way.

One first must ask what physical terms we would expect the drag to have a dependency on. We would expect some dependency on the velocity  $v$  of the object through the fluid, on the shape of the body and a characteristic length scale  $r$  for the body, on the density of the fluid  $\rho$ , and finally on the viscosity of the fluid  $\nu$ . As noted in [Jensen \(2013\)](#) we have no dependency from the mass of the body on the drag. As per the rest of this project we also assume the fluid is incompressible.

Forming an equation in the style of [\(2.2.4\)](#) between these quantities and the drag force  $D$  we obtain

$$D = g v^\alpha r^\beta \rho^\gamma \nu^\delta \quad (2.2.7)$$

where  $g$  is a dimensionless constant which will take into account the shape of the body and potentially other dimensionless parameters such as the Reynolds number [\(2.2.5\)](#).

We attempt to obtain values of  $\alpha, \beta, \gamma, \delta$  which balances [\(2.2.7\)](#). The dimensions of the quantities in [\(2.2.7\)](#) are as follows:

$$[D] = MLT^{-1}, \quad [v] = LT^{-1}, \quad [r] = L, \quad [\rho] = ML^{-3}, \quad [\nu] = ML^{-1}T^{-1}$$

and so balancing [\(2.2.7\)](#) implies that

$$MLT^{-2} = M^{\gamma+\delta} L^{\alpha+\beta-3\gamma-\delta} T^{-\alpha-\delta}. \quad (2.2.8)$$

Equating the powers leads to a system of 3 linear equations in 4 variables for each

fundamental unit given by

$$1 = \gamma + \delta \quad (2.2.9a)$$

$$1 = \alpha + \beta - 3\gamma - \delta \quad (2.2.9b)$$

$$-2 = \alpha - \delta \quad (2.2.9c)$$

for  $M$ ,  $L$  and  $T$  respectively.

Using these equations we can eliminate all but one of the parameters, and writing all these in terms of  $\delta$  we can find

$$D = g v^{2-\delta} r^{2-\delta} \rho^{1-\delta} \nu^\delta \quad (2.2.10)$$

and rearranging these powers

$$D = g \rho r^2 v^2 \left( \frac{\nu}{\rho r v} \right)^\delta. \quad (2.2.11)$$

We can then recognise that the term in the brackets is  $1/Re$ . Following [Jensen \(2013\)](#) we can derive, using a similar analysis, that  $g$  must also have some functional dependency on the Reynolds number, and as such

$$D = \rho r^2 v^2 f(Re). \quad (2.2.12)$$

The form of  $f$  depends on the velocity of the body moving through the fluid.

In the low velocity limits of low and high velocity we find slightly different forms for the dependence on velocity. In the low velocity limit, the dependency on velocity is only linear, that is

$$D = g \nu r v. \quad (2.2.13)$$

where  $g$  is simply related to the shape of the body. This is known as stokes drag, corresponding to laminar flow about the body. Whereas in the high velocity limit we would expect turbulent flow behind the body. This is the case which manifests during the flight of a golf ball, and the distinction will be important later.

$$D = g \rho r^2 v^2 \quad (2.2.14)$$

On comparison with [\(2.2.12\)](#) we see that at low velocity,  $f(Re) \propto Re^{-1}$  and in the high velocity case  $f(Re)$  is independent of  $Re$ .

Within the literature related to fluid dynamics and aerodynamics (2.2.14) is normally written with different names for the variables, namely

$$F_D = \frac{1}{2}\rho\mathbf{V}^2 A_{c_D} \quad (2.2.15)$$

where  $F_D$  is the drag force, and  $c_D$  is the dimensionless drag coefficient. Is it this form we will use from here on.

An expression for the lift can be derived using very similar analysis, and has the same form as the drag:

$$F_L = \frac{1}{2}\rho\mathbf{V}^2 A_{c_L} \quad (2.2.16)$$

where here  $c_L$  is the lift coefficient.

## 2.2.5 Boundary Layer Separation and the Magnus Effect

In addition to the drag forces which we have discussed in the previous section, there is another major effect from the motion of the fluid on golf ball trajectories: the Magnus effect. The Magnus effect is caused by the spin of the ball moving through the fluid medium, and accounts for large deviations from a trajectory not considering the effect Seifert (2012).

In the Magnus effect, the boundary layer around the spinning body separates (in some literature this is called detaching instead) from the body and forms a wake behind the body.

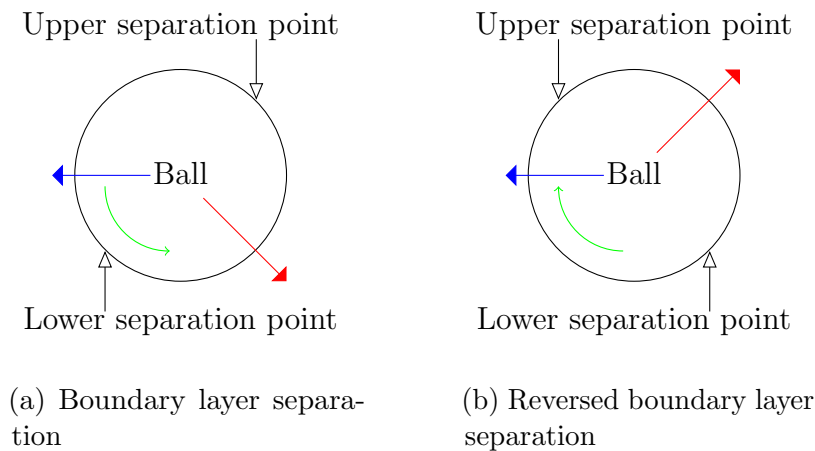


Figure 2.1: Here we see the two scenarios for boundary layer detachment. The red arrow indicates the direction which the detached boundary layer proceeds in, the blue arrow the direction of the ball, and the green arrow the direction of spin of the ball.

The points at which the boundary layer separates from the body at the top and bottom of the ball make a significant difference to the direction in which the wake will point: if the boundary layer at the top of the ball separates later than the bottom (see a in Figure 2.1) then we will have a positive Magnus effect, and the lift will be increased. In the opposite case, where the bottom separates later than the top, we will have a negative Magnus effect (see b in Figure 2.1) and the lift on the ball will be decreased or potentially act to push the ball further towards the ground.

The fluid behind the rotating sphere will become turbulent as the sphere leaves a gap which the wake refills as it passes. This mechanism is important while modelling the golf ball later, as the size of the turbulent wake will affect the drag on the ball.

The streamlines over the ball can be visualised as such

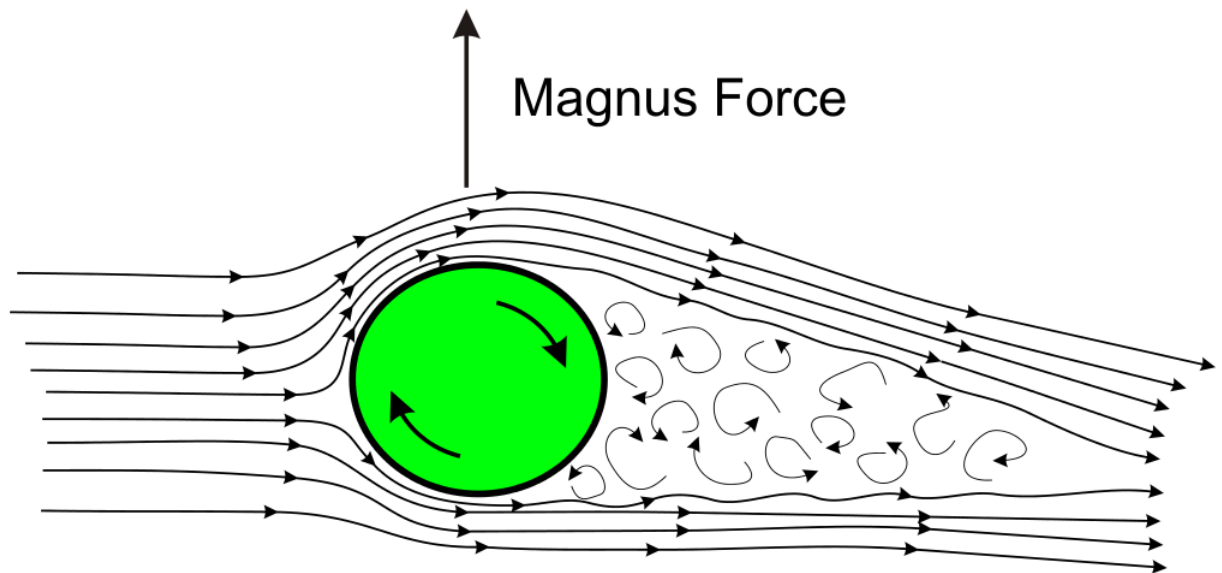


Figure 2.2: A diagram of the Magnus force on a rotating sphere. Adapted from [http://en.wikipedia.org/wiki/File:Sketch\\_of\\_Magnus\\_effect\\_with\\_streamlines\\_and\\_turbulent\\_wake.svg](http://en.wikipedia.org/wiki/File:Sketch_of_Magnus_effect_with_streamlines_and_turbulent_wake.svg).

In this diagram we have lamina flow in the boundary layer over the ball. However, this is not always the case: when the flow becomes turbulent the drag can change considerably.

### 2.2.6 The Drag Crisis

When measuring the flow around a smooth sphere, one finds a curious phenomenon. At approximately  $Re = 2 \times 10^5$  the drag coefficient on the sphere suddenly decreases

from around  $c_D = 0.4$  to  $c_D = 0.1$ . This sudden change in drag is associated with the boundary layer around the sphere becoming turbulent and the wake behind the ball, as described before, becoming shorter and thinner as compared to the size of the ball.

Modelling this transition to turbulence is incredibly difficult, even for smooth spheres, and is incredibly difficult for the case of a dimpled golf ball. While there are some hints towards progress in finding analytic solutions for this transition to turbulence for a smooth sphere [Assis et al. \(2010\)](#), we must make do with measurements from experiments to get some idea of how this works.

In [Morrison \(2010\)](#) all experimental data for the drag on a smooth sphere is combined to give a formula for the drag in the Reynolds number range  $Re = 1$  to  $Re = 10^6$ . This combined form exhibits the drag crisis drop at around  $Re = 2 \times 10^5$  experiments have seen, and is given by

$$c_D = \frac{24}{Re} + \frac{2.6(Re/5)}{1 + (Re/5)^{1.52}} + \frac{0.411(Re/263000)^{-7.94}}{1 + (Re/263000)^{-8.00}} + \frac{Re^{0.8}}{461000}. \quad (2.2.17)$$

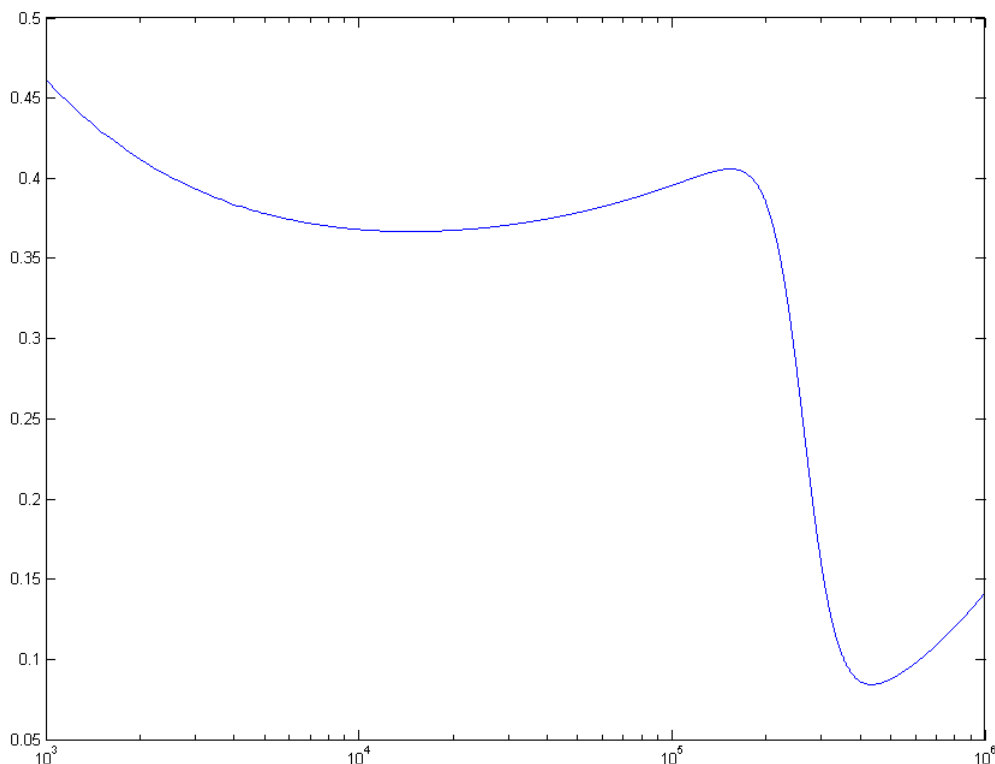


Figure 2.3: A plot of the Morrison drag formula from  $Re = 10^3$  to  $Re = 10^6$ . Note the sudden drop in drag at around  $Re = 2 \times 10^5$  as expected.

For a golf ball, the presence of dimples on the surface of the ball serves to reduce the Reynolds number at which the drag crisis occurs [Alam et al. \(2011\)](#), moving the



range of speeds where the golf ball is in the low drag (supercritical) region to within the capability of a human golfer to hit. This vast reduction in drag makes a large difference to the flight of a ball, and we will need to account for this affect in any model we form.

The configuration of the dimples on the ball also has a large effect on the values of  $Re$  at which the drag crisis occurs, and the value of  $c_D$  at either side of the drop [Naruo and Mizota \(2014\)](#). There is a large variation between particular type of ball (see Figure 3 in [Naruo and Mizota \(2014\)](#)), which mean that individual balls can likely be characterised simply in terms of their drag function.

## 2.3 Previous Work on Modelling Golf Ball Flight

There has been considerable attention within the literature on the topic of modelling the flight of a golf ball, both due to the considerable industry surrounding the game and the interesting fluid dynamics which results from golf ball flight. A small selection of such papers are [Smits and Ogg \(2004\)](#); [Bearman and Harvey \(1976\)](#); [Penner \(2003\)](#); [Alam et al. \(2011\)](#); [Kensrud and Smith \(2010\)](#); [Leong and Lin \(2007\)](#) however there are many more which could be discussed.

The earliest of these papers is [Bearman and Harvey \(1976\)](#) which is one of the first attempts to understand the fluid dynamics over a golf ball and provide a model for the flight of a ball taking this into account. The drag crisis on a golf ball is shown in experimental data taken from an earlier paper and from measurements the authors made in a wind tunnel. These measurements were taken at a range of  $Re$  values and spin values, providing a useful set data to correlate any findings against. The paper also emphasizes the importance of the dimples on the aerodynamic characteristics of the ball, in agreement with other papers.

In [Smits and Ogg \(2004\)](#) the authors summarise the main effects one will find on golf ball trajectories, mentioning both the laminar and turbulent boundary layer we discussed previously, the effect of spin on the lift coefficient, and including some of the data from [Bearman and Harvey \(1976\)](#) to illustrate these points. The paper also suggests that much work still remains in understanding how the fluid dynamics over golf balls functions, saying that fundamentally balls are designed via empirical means, simply using the knowledge contained in the previous sections and experiments to

improve the designs of balls. The authors state also state, with reference to the design of golf balls [Smits and Ogg \(2004, page 10\)](#):

“The fundamental design challenge in optimizing golf ball aerodynamics is achieving the lower possible drag level at high Reynolds number while ensuring a high lift coefficient at the lowest Reynolds number in the design space.”

These two goals are virtually at opposite ends from each other and thus means the challenge of making a good golf ball for all ranges of speed in a typical game is very difficult.

There are a number of papers exclusively on experimental measurements of drag and lift on golf balls, for example [Kharlamov et al. \(2007\)](#), [Naruo and Mizota \(2014\)](#), [Kray et al. \(2012\)](#) and [Aoki et al. \(2010\)](#). All of these papers show evidence for the drag crisis at lower Reynolds number than a smooth sphere, and for the Magnus effect on on flight. [Aoki et al. \(2010\)](#) gives a value for the transition to the supercritical drag regime as  $Re = 0.5 \times 10^5$  which is slightly lower than the values given in other references. However, this can be accounted for by noting that this measurement is taken without rotation and potentially with a different ball to other references. Additionally, this paper contains direct measurements of the boundary layer separation on both sides of a rotating ball, and finds excellent agreement between the expected behaviour and the real physical behaviour.

[Kray et al. \(2012\)](#) focuses on the Magnus effect predominantly, and takes experimental measurements on larger spheres than a golf ball. However, these measurements are in a similar Reynolds number range to the case for golf and so the results here could be of some use. The authors also report observing the negative Magnus effect in their tests. However, some of the results within in this report are obtained using a sphere attached to two rods in a wind tunnel which could significantly affect the fluid flow in the boundary layer, a point the authors themselves concede.

Finally, in [Naruo and Mizota \(2014\)](#) the effects of differing the depth of the dimpling on a golf ball is explored at a range of flow speeds. The authors find that even small changes to the dimple configuration (a change in depth of 0.035mm) can have large effects on the lift on the ball and thus the resultant trajectory. Additionally, the authors attempt a strategy with a ball with smaller dimples placed between the normal sized dimples a standard golf ball. They report a increase in the carry of the ball of

approximately 8m. While we will not investigate into the dimpling on the ball, it is interesting to see the directions that golf ball technology may advance in in the future.

### 2.3.1 Computational Simulations of Golf Ball Flight

Performing accurate computational simulations of the flow over a golf ball is a particularly large challenge. The complex turbulent wake behind a golf ball, and the potential for the turbulent boundary layer, along with the rotation and high Reynolds numbers the flow typically operate in mean that any computational simulations will need both small time stepping and large mesh sizes to deal with the resultant flow.

It is only recently that such simulations have become feasible using super computers with large numbers of cpu cores and memory. Parallelisation of these methods means that systems with large numbers of cpu cores can dramatically cut down the time that such simulations take.

The first paper to attempt a full simulation of the flow over a non spinning ball for a range of Reynolds numbers was [Smith et al. \(2010\)](#). The authors use a fairly sophisticated discretisation method for the points within the domain, dividing them into interior points within the ball, forcing points directly on the boundary which have different boundary conditions, and fluid points. Each of these has different behaviour to the other, and some interpolation methods are used to bridge the gap between the values at each set of points. This methodology is used as the points do not have to fit around the boundary of the ball, allowing a much simpler Cartesian grid to be used instead of attempting to use a grid set in a spherical coordinate system with the ball.

The solution is based on solving the full Navier Stokes equations, [\(2.2.2\)](#) and [\(2.2.3\)](#) around the golf ball for the flow, using a Crank-Nicholson method for the viscous terms and using a third order Runge-Kutta scheme for the other terms. The ball modelled has 300 dimples, a fairly typical configuration.

The results are in good line with the behaviour we expect to see for Reynolds numbers between the subcritical (here  $Re = 2.5 \times 10^4$ ) and supercritical ( $Re = 1.1 \times 10^5$ ) regimes, finding the drag crisis drop that experiments have observed. The authors also obtain visualisations of the flow over the ball in the two different regimes, finding the transition to turbulence in the boundary layer in the supercritical range and the turbulent wake behind the ball.

[Beratlis et al. \(2012\)](#) extends this work to spinning golf balls, and samples from a different set of Reynolds number, this time in the subcritical domain  $Re = 1.7 \times 10^4$ , during the critical Reynolds number drop  $Re = 4.5 \times 10^4$  and  $Re = 6.5 \times 10^4$ , and in the supercritical section at  $Re = 1.7 \times 10^5$ . This study uses a more sophisticated grid setup in cylindrical coordinates, with a similar hybrid explicit and implicit scheme to solve the Navier-Stokes equations around the ball.

The computational resources used within this study are quite considerable: as the lower Reynolds number the grid size is approximately  $3 \times 10^7$  points, and the authors estimate that each rotation takes 1800 hours of cpu time to compute. By the final Reynolds number, and at highest spin, the grid is increased by over 5 times to approximately  $1.5 \times 10^8$  points, and the authors estimate this takes 260000 hours of cpu time to compute.

These investigations find a similar result to both the experiments and the previous work in [Smith et al. \(2010\)](#), seeing all the features we would expect and following the experimental data quite closely.

Finally, in [Aoki et al. \(2010\)](#) some numerical simulations of the flow using the FLUENT fluid dynamics software is undertaken. The authors only obtained a few results, and crucially only one result after the advent of the drag crisis. While the results they find are broadly within line with the expected experimental results there are too few to really validate the accuracy of the technique.

Using computational fluid modelling over golf balls is still in its infancy, and there is a long way to go until the technique is sufficiently accurate to be able to easily model different types of ball. The huge computational resources required are a problem, however as computers grow more powerful and generally have more cores this will come within the range of researchers to quickly simulate the flow over a ball.

## 2.4 Measuring Golf Ball Trajectories

Golf ball trajectories can be measured in a number of ways, depending on the distance over which we wish to take the measurements. There are setups over small ranges which use cameras to track the ball during its flight, however these are limited in the range at which the ball can be distinguished by the camera.

In this project, the data we have been supplied with predominantly uses Doppler radar to measure the full trajectory of the flight. This allows both the position of the ball over the flight to be found and the spin, by virtue of the use of the Doppler effect to measure the rotational motion of the ball.

It is possible to also use this Doppler radar technique to estimate the  $c_D$  at each point of the flight, as is described in [Martin et al. \(2012\)](#) for the case of baseballs.

# Chapter 3

## A Model of Golf Ball Flight

The motion of a golf ball can fundamentally be viewed as a set of forces acting on the ball as it flies through the air. Before we can obtain a better understanding of the nature of the drag and lift, or characterise a ball by the lift and drag functions we find, obtaining a model for the forces acting on the ball during the flight is advisable.

Here, we follow the paper by [Robinson and Robinson \(2013\)](#), which builds a model of the flight based on simple principles as we desire. This model does neglect some of the subtlety of the fluid dynamics we have discussed, but is a useful starting point for the analysis.

### 3.1 A Model for Golf Ball Flight

In [Robinson and Robinson \(2013\)](#) the authors first discuss the assumptions and limitations of the model at hand. We will take the reverse to this approach, discussing the features of the model and then mentioning some of the potential improvements to the model and the drag and lift form they give.

Additionally, the authors give a sample MATLAB script for the setup of the differential equations they derive and suggest using MATLAB to solve the resultant differential equations of the model numerically. This sample code forms the bases of our initial investigations into the trajectories.

#### 3.1.1 Lift and Drag

[Robinson and Robinson](#) start by initially discussing the lift and drag forces on a golf

ball. They use the form of the lift and drag in the high Reynolds number limit, given by

$$F_D = \frac{1}{2}\rho\mathbf{V}^2Ac_D$$

and

$$F_L = \frac{1}{2}\rho\mathbf{V}^2Ac_L$$

The use of this form of equation is justified by the authors stating that there is experimental evidence that golf ball flight always occurs at  $Re > 10^3$ . We will examine this assumption later.

### Drag

The authors give a form for  $c_D$  based on the spin of the ball

$$c_D = 0.3 + 2.58 \times 10^{-4}\omega \quad (3.1.1)$$

where  $\omega$  is the modulus of  $\vec{\omega}$  the spin vector, in radians per second. This is obtained from experimental results found by [Davies \(1949\)](#). However, the authors elect to take  $c_D = 0.45$ , rationalising that this simplification is most suited to the range of spins and speeds which golf balls are likely to take. The authors also mention the lack of experimental evidence they found to suggest better forms for  $c_D$ .

### Lift

[Robinson and Robinson](#) make the following assumptions for the lift on the golf ball:

- The direction of the lift for is perpendicular to both  $\omega$  and  $\mathbf{V}$ , that is  $\vec{F}_L \propto \omega \times \mathbf{V}$ .
- The lift is not a function of the drag.

They then go on to express the lift force as a vector quantity, given by

$$\vec{F}_L = \frac{1}{2}\rho Ac_L V^2 \sin \theta \cdot \hat{n} \quad (3.1.2)$$

and then using the definition of cross products rewrite this as

$$\vec{F}_L = \frac{1}{2}\rho Ac_L V \cdot \left( \frac{\vec{\omega} \times \mathbf{V}}{\omega} \right) \quad (3.1.3)$$

which is the form used in the model.

As with  $c_D$ , the authors then use experimental data to inform their choice for  $c_L$ , once again following [Davies \(1949\)](#) to find that

$$c_L = 3.19 \times 10^{-1} (1 - \exp(-2.48 \times 10^{-3} \omega)) \quad (3.1.4)$$

fits with a number of different experimental studies of the lift over spheres.

The authors also state that this form completely omits any possibility of a negative Magnus effect pushing the ball towards the ground.

### 3.1.2 Accounting for the Wind

In order to deal with the effect of the wind on the golf ball the authors introduce a new  $\vec{v}$  which is defined as being the velocity of the ball relative to the air. That is, if the wind is blowing with a velocity  $\vec{W}$  and the ball moving with velocity  $\mathbf{V}$  with respect to the coordinates then the ball is moving with velocity  $\vec{v} = \mathbf{V} - \vec{W}$  with respect to the air.

### 3.1.3 The Equations of Motion

By considering a force balance on the golf ball in flight, the authors obtain

$$m\ddot{\vec{r}} = -\frac{1}{2}\rho A c_D |\mathbf{V} - \vec{W}| (\mathbf{V} - \vec{W}) + \frac{1}{2}\rho A c_L |\mathbf{V} - \vec{W}| \left( \frac{\vec{\omega} \times (\mathbf{V} - \vec{W})}{\omega} \right) + m\vec{g}. \quad (3.1.5)$$

Where  $\vec{r}$  is the position vector from the origin, taking the  $z$ -axis to be facing upwards, and  $x$  and  $y$  in the plane with the ground. The dot here means the time derivative. The three terms here are coloured by their origin:

- In blue is the drag term accounting for the action of the wind.
- In green is the lift term, written in terms of cross products, accounting for the action of the wind.
- In yellow is the action of gravity on the ball, with  $\vec{g} = (0, 0, -g)^T$ .



If we write these into their respective components we obtain, expanding the cross product terms into the components of vectors

$$m\ddot{x} = -\frac{1}{2}\rho A|\mathbf{V} - \vec{W}| \left( c_D(V_x - W_x) - c_L \frac{\omega_y(V_z - W_z) - \omega_z(V_y - W_y)}{\omega} \right) \quad (3.1.6a)$$

$$m\ddot{y} = -\frac{1}{2}\rho A|\mathbf{V} - \vec{W}| \left( c_D(V_y - W_y) - c_L \frac{\omega_z(V_x - W_x) - \omega_x(V_z - W_z)}{\omega} \right) \quad (3.1.6b)$$

$$m\ddot{z} = -\frac{1}{2}\rho A|\mathbf{V} - \vec{W}| \left( c_D(V_z - W_z) - c_L \frac{\omega_x(V_y - W_y) - \omega_y(V_x - W_x)}{\omega} \right) - mg. \quad (3.1.6c)$$

In order to solve these equations we rewrite them into a set of 6 first order equations, instead of three second order ones, as

$$\dot{\vec{r}} = \vec{v} \quad (3.1.7a)$$

$$m\dot{\vec{v}} = -\frac{1}{2}\rho A c_D |\mathbf{V} - \vec{W}| (\mathbf{V} - \vec{W}) + \frac{1}{2}\rho A c_L |\mathbf{V} - \vec{W}| \left( \frac{\vec{\omega} \times (\mathbf{V} - \vec{W})}{\omega} \right) + m\vec{g} \quad (3.1.7b)$$

This rewriting allows an implementation of the equations which may be solved using the standard differential equation solvers within MATLAB.

Solving these equations involves giving 6 initial conditions: the three coordinates at the start of the trajectory and the components of the initial velocity.

### 3.1.4 An Example Trajectory

In order to show this model working, we will demonstrate solving an example problem in matlab with values taken from a trajectory provided by The R&A.

Here, we take the following initial conditions

$$x = 0, \quad y = 0, \quad z = 0, \quad v_x = 68.221, \quad v_z = 12.701, \quad v_y = -4.961.$$

and the components of the wind to be negligible (setting all the components to zero).

In figure 3.1 we plot the range ( $x$ -axis) against the height of the the golf ball during the flight. There are several encouraging features within this plot: the height and range are within the bounds set by considering the ball as a projectile and completely negating the affect of drag, and the shape of the trajectory is not simply that of a parabola, implying that the lift and drag are changing how the ball flies.

In figure 3.2 we display a 3 dimensional plot of the trajectory. Here we notice that the spin of the ball influences the movement in the  $y$  plane fairly considerably, adding

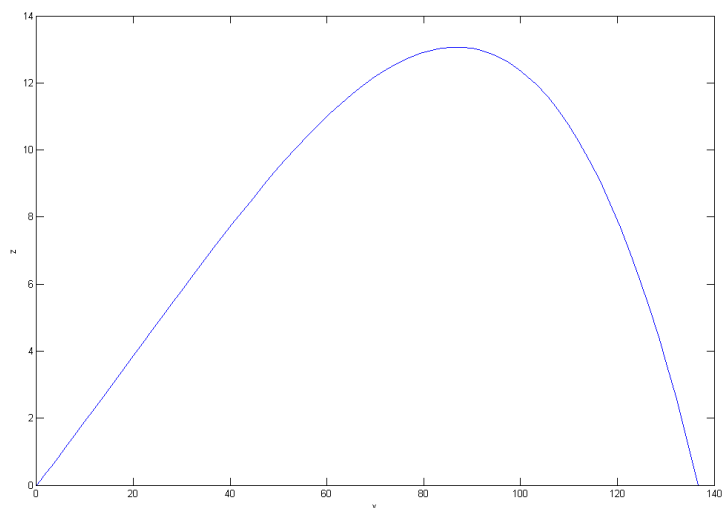


Figure 3.1: Here we plot the distance of the golf ball against the height, using the basic Robinson and Robinson model to calculate the trajectory.

a deviation from a standard projectile which we would not predict by projectile motion alone. This is the action of the spin on the trajectory.

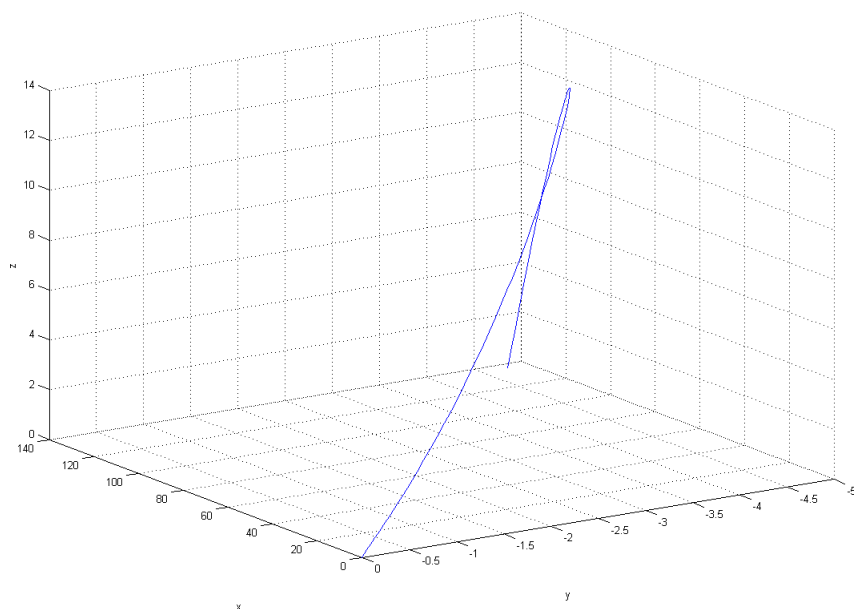


Figure 3.2: A 3D plot of the same model as Figure 3.1, showing the deviation due to the spin of the ball in this model.

## 3.2 Limitations of the Model

While the model given by [Robinson and Robinson \(2013\)](#) is a good start, it is not without flaws. The authors themselves admit that there are a number of points where the model could potentially be improved

- The model only takes into account a positive Magnus effect, but if the separation points were to move to a different position on the ball this form would no longer apply.
- The constant value of  $c_D$  is rather troubling, particularly considering there is some experimental evidence that the golf ball does reach the critical and supercritical domain during the course of an average golf ball flight.
- The form of  $c_D$  and  $c_L$  have no dependency on Reynolds number at all, which contradicts previous analysis.
- The spin of the ball is assumed constant throughout the flight. The authors state that in most situations the loss of spin is low enough to be ignored, citing some evidence that the ball keeps a significant proportion. This assumption is also presented in [Lieberman and Smits \(2001\)](#), where the simple differential equation

$$\dot{\omega} = -0.00002$$

is used to model the spin decay. This constant is so small as to cause almost no change in spin over the flight, and as such we will not concern ourselves with modelling spin decay.

The authors do state, however, that building dependency on speed and spin into their model would be possible with the analysis they have performed, allowing these limitations to be addressed without drastically changing the form of the resultant equations.

The lack of any dependency on speed is addressed within [Jensen \(2014\)](#) by means of dimensional analysis. Jensen uses a similar analysis to the previous section on drag to determine that if  $c_L$  is independent of the Reynolds number then it cannot, by dimensionality arguments, only be a function of  $\omega$ . Instead, in order for the function to have some dependency on spin a possible dimensionless grouping of  $r\omega/\mathbf{V}$  can be

used. Jensen also suggests several other forms which  $c_D$  and  $c_L$  may take based solely on dimensional considerations.

Robinson and Robinson (2014) is the authors of Robinson and Robinson (2013) reply to the paper by Jensen. Robinson and Robinson state that the second constant in (3.1.4), as found from Davies (1949), is given in units of  $1/(\text{rad s}^{-1})$ , and as such cancel with the units of  $\omega$  and overall give an expression which is dimensionless, as we expect  $c_L$  to be from our earlier discussion. The authors go on to discuss the necessity and normality of having a multiplying constant which renders an expression dimensionally consistent, giving an example based on the spring constant from Hooke's Law.

Robinson and Robinson also give a number of other references to experimental data confirming their assumptions with regards to the dependency of lift on spin, and discuss some other alternative forms of the lift force with different dependencies on the velocity of the ball.

### 3.2.1 Comparing Trajectories with Data

In order to improve upon the model by Robinson and Robinson the first thing to do is attempt to validate the trajectories generated against data provided by The R&A, and hopefully obtain some understanding of which model assumptions are incorrect.

If we use the same initial conditions as in section 3.1.4 and plot this against a trajectory provided by The R&A using their Doppler radar system we obtain Figure 3.3. We note that the model under predicts the height and range of the ball by a considerable degree.

In Figure 3.4 a 3D plot of this data is shown. Here we see that the model initially shows good agreement with the data but as the ball approaches the top of the flight the model and the data deviate considerably from each other, with the actual trajectory curving back towards the  $y = 0$  line. This effect is completely absent from the curve given by the Robinson and Robinson model and suggests that the drag or lift need significant changes in order to fit with the data.

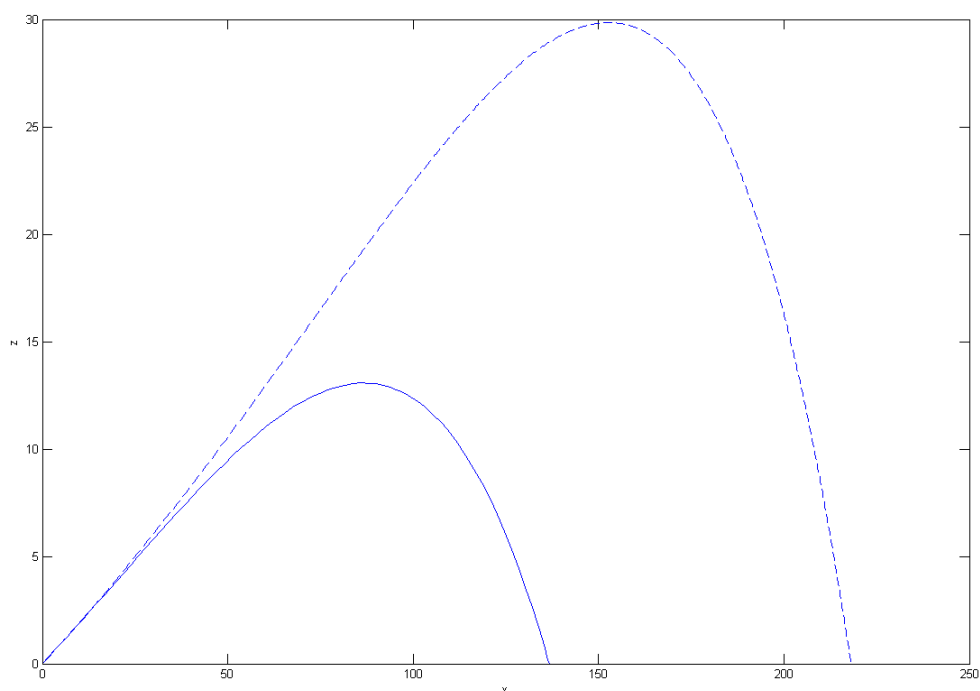


Figure 3.3: Here we plot the Robinson and Robinson model in blue against data provided by The R&A in a dashed line. The significant change in maximum height and carry of the ball highlight the fact that there are significant improvements to be made to the model.

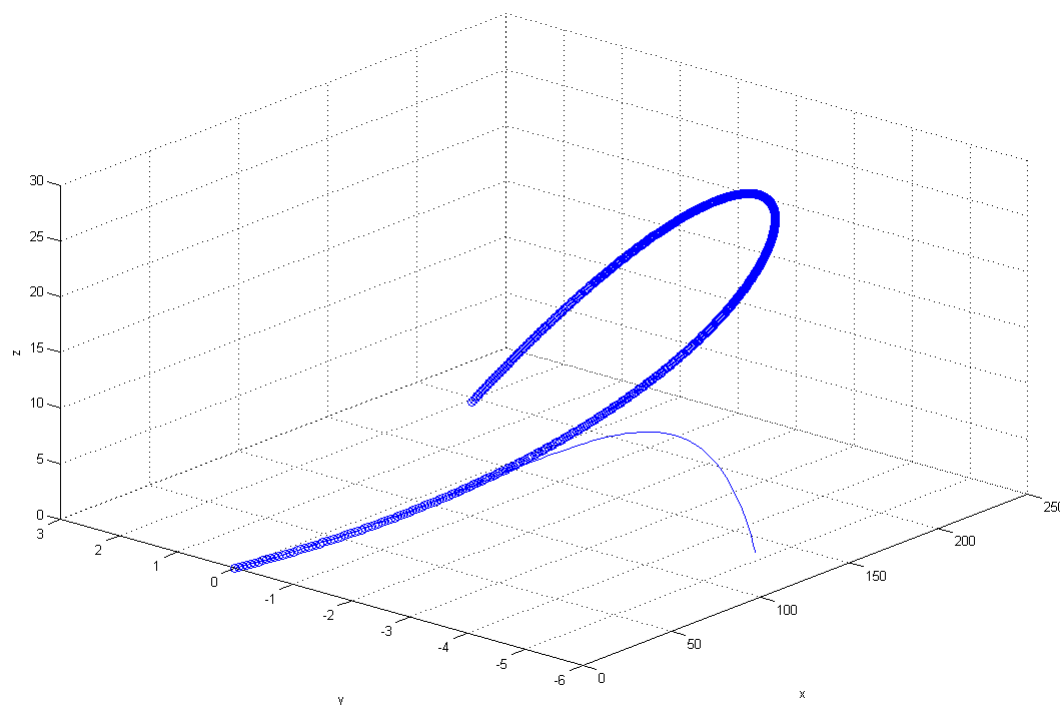


Figure 3.4: Here we plot the Robinson and Robinson model in blue against data provided by The R&A plotted with blue circles. While the model initially fits the data well, as the ball approaches the top of the flight the two curves deviate significantly.

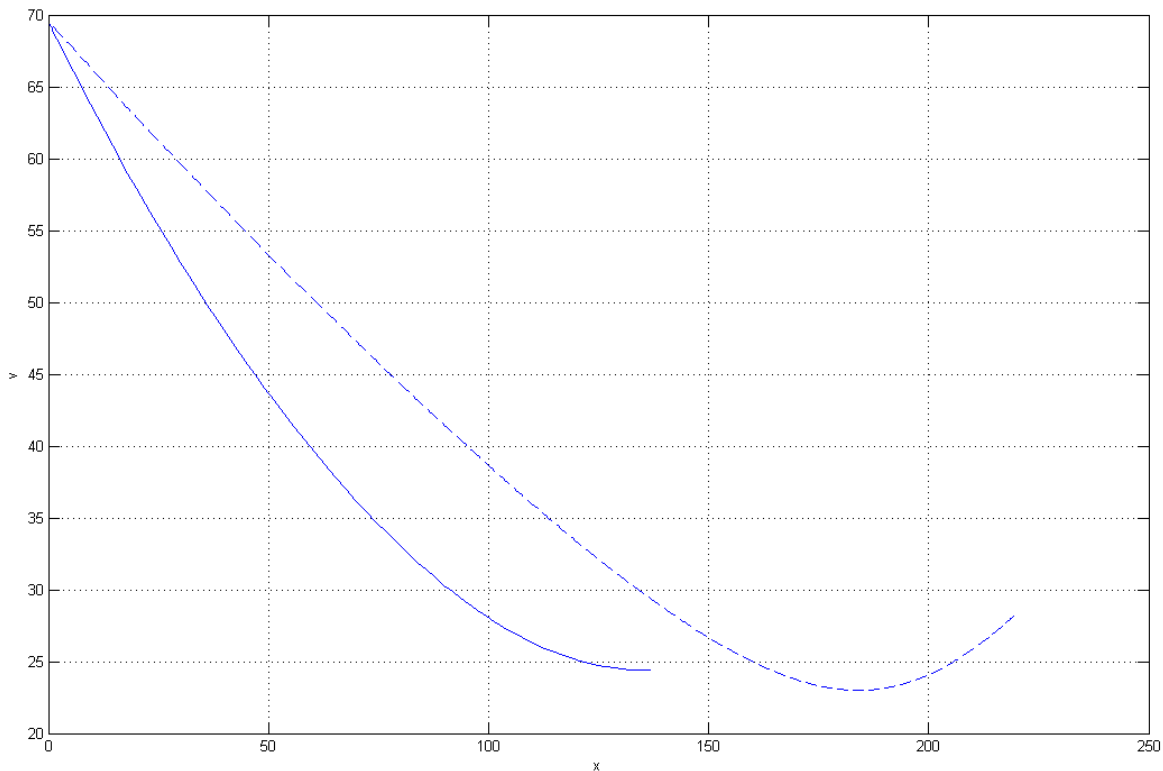


Figure 3.5: Here we plot the speed of the projectile in solid line against the speed as measured by the radar in dashed line. Note that while the curves start with the same initial condition they quickly deviate from each other.

One hint as to the failings of this model is to plot the speed of the speed of the projectile against the distance along the  $x$ -axis, as in Figure 3.5. We see that while the curves start together, they immediately deviate from each other. By  $x = 50$  the Robinson and Robinson model predicts the speed to be  $10\text{m s}^{-1}$  less than the speed obtained from the data.

On calculating the Reynolds number for the flight, at the start of the trajectory the Reynolds number is approximately  $1.6 \times 10^5$ , which is just where we believe the supercritical regime begins. This would invalidate the assumption which Robinson and Robinson make that the drag is likely to be nearly constant through the entire motion of the projectile. Instead, the drag on the ball must initially be very different to the value which Robinson and Robinson assumes it to be throughout the flight. This difference accounts for the variation of the speed of the ball immediately after being hit, as the drag on the real ball will be much less than the drag in the model, slowing the ball less and keeping the ball in the critical or supercritical Reynolds numbers for longer.

### 3.3 Improvements

[Robinson and Robinson \(2013\)](#) give fairly well justified reasons to take the lift to be in the form they suggest including referencing a number of experimental results that fit well with the form they give. Thus, we will focus our investigations primarily on finding a better form for the drag function on the ball, as this will likely yield the biggest improvements to the model.

The assumption that the ball never reaches the supercritical Reynolds numbers appears, by investigation of the data above (and from other data sets obtained from The R&A) seems to be false, so finding a functional form of  $c_D$  which takes into account the drag crisis for Reynolds numbers within the range encountered during golf ball flight is a good starting point for investigations.

# Chapter 4

## Improving $c_D$

If we are to be able to estimate the trajectories based on the initial conditions successfully, we need to be able to reliably solve the forwards problem for the trajectory of the golf ball. In order to do this, as stated at the end of the previous chapter, we must find an improved form for  $c_D$  which more accurately describes the physics which occurs during the flight of a ball.

There are a number of approaches to this, and we have attempted a few of them in our investigations in an attempt to find which of them gives the most reliable results. Any model of golf ball flight which captures the dynamics of an individual ball will have to use flight data to inform the exact parameters in a drag function for that ball. Thus, much of this chapter is also concerned with attempting to find methods of estimating the parameters for such functions given data on the flight of a particular ball.

This parameter estimation is an example of an inverse problem. Some generalities on such problems are given in the appendix.

### 4.1 Estimating $c_D$ from Experiments

As a first attempt at estimating  $c_D$ , we began by returning to the form given in [Morrison \(2010\)](#) and discussed in section [2.2.6](#). Recalling that we expect the dimpled surface of the golf ball to have the affect of moving the point at which the drag crisis occurs to lower Reynolds numbers, we began by taking Morrison’s form for the drag and attempting to change the coefficients to “move” the drop in drag to within the range seen within experiments on golf balls.



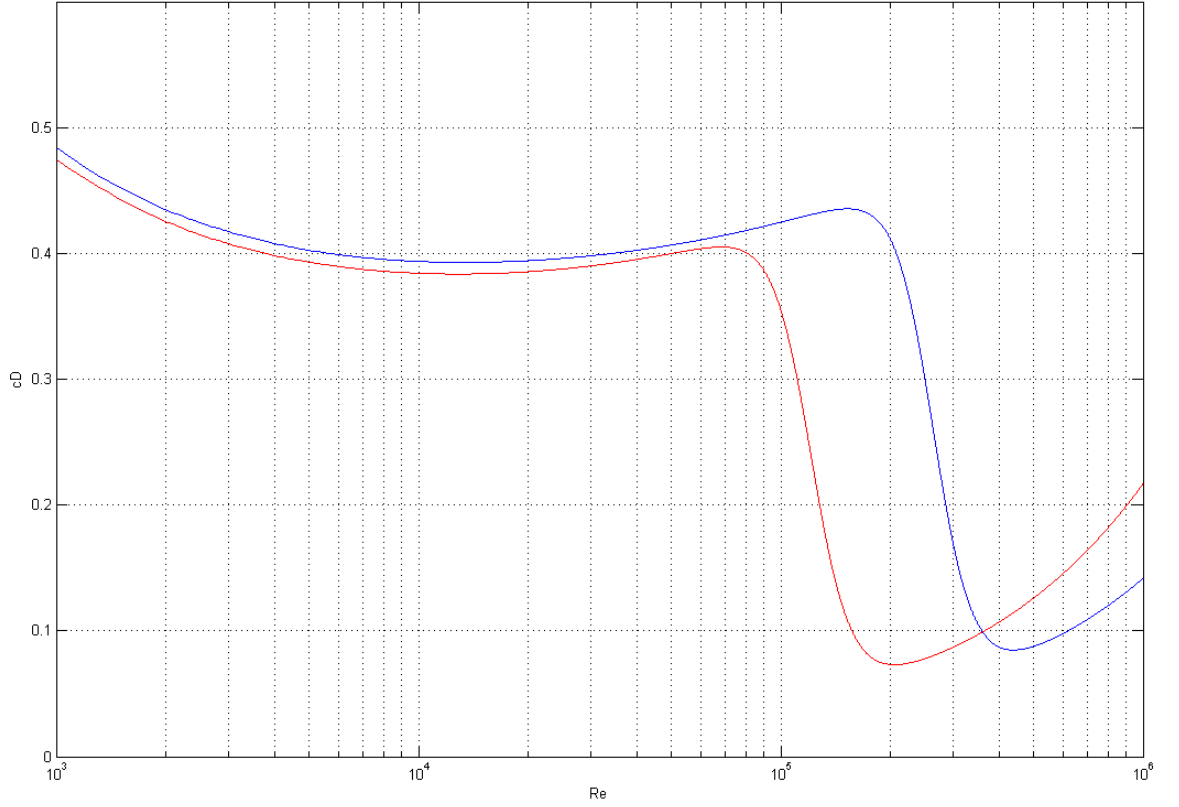


Figure 4.1: In blue is the original  $c_D$  function, given in (2.2.17). In red is the modified form, (4.1.1), which takes into account the lower value of Reynolds number where the transition to lower drag occurs.

Here, we attempt to match the function to the experimental data given in various papers which we have listed before. After some consideration, the following form of  $c_D$  can be found to fit with a number of different experiments

$$c_D = \frac{24}{Re} + \frac{2.6(Re/5)}{1 + (Re/5)^{1.52}} + \frac{0.38(Re/121000)^{-7.94}}{1 + (Re/121000)^{-8.00}} + \frac{Re^{0.83}}{450000}. \quad (4.1.1)$$

We believe that this form captures the physics we expect to see from the golf ball better than simply taking a constant value of  $c_D$  as in Robinson and Robinson (2013). Plotting the original and the modified form of  $c_D$  shows how the drag has moved to within the range we expect to see.

This form has a number of limitations, but does serve to be a good initial start at working out the drag for a golf ball. The weaknesses can be summarised as

- This form of  $c_D$  is constant for all types of golf balls, which we know is not the case for realistic balls, as noted in Alam et al. (2011).
- Changing this function for different balls is a matter of hand choosing coefficients

in the terms of (4.1.1). This method is not at all easy to modify for other balls.

- While the form of  $c_D$  is dimensionless, as we require it to be, there is no dependence on spin at all, which could be causing significant contributions to the drag.

Replacing  $c_D$  in the model by Robinson and Robinson by  $c_D$  as defined in (4.1.1) does make a significant change to the resultant trajectory, bringing the height of the ball much closer to the experimental trajectories and improving the carry of the ball significantly.

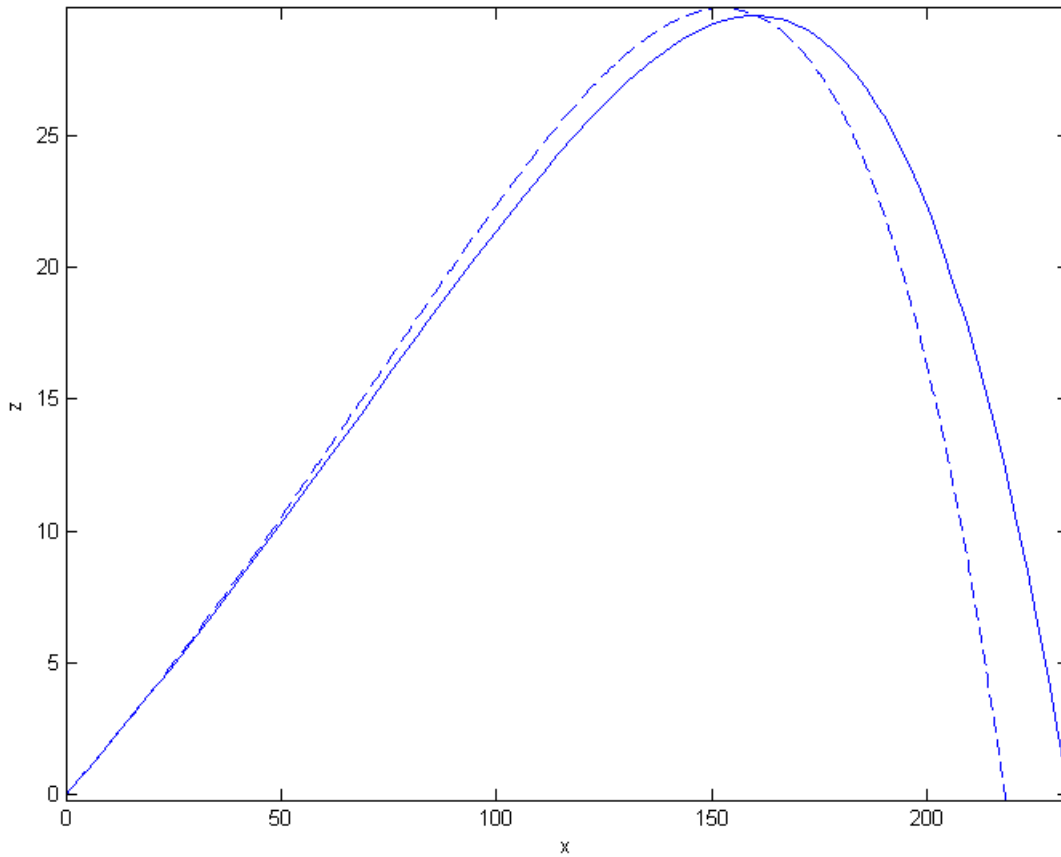


Figure 4.2: Using the modified Morrison form for  $c_D$  results in a fairly accurate profile. Here the solid line is the model prediction and the dashed line is the data.

In Figure 4.2 we see that this form of the drag function brings the model and experimental results into close agreement with each other. However, viewing the trajectory in 3D reveals that while the height and carry of the ball are predicted well, the motion along the  $y$  axis is not predicted as well, deviating by approximately 5m at the end of the trajectory.

While we see good agreement between the model and the data for this data set,

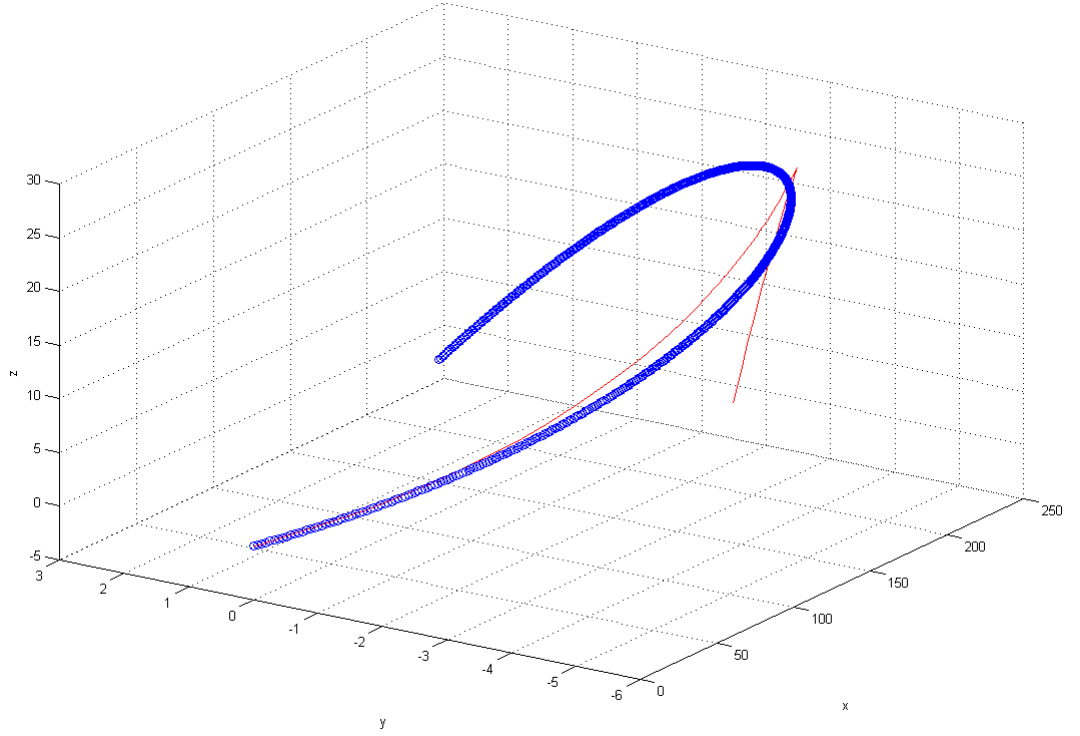


Figure 4.3: This is a 3D plot of Figure 4.2. We note that initially the predicted curve fits the data almost perfectly, being within 1m. Just before the apex of the curve however the data (plotted with circles) veers back towards the  $y = 0$  line, whereas the model (in red) does not have this behaviour.

running the model with a different set of initial conditions and using data taken with a different ball does not yeild such close agreement.

The R&A provided another data set, this time with 4 trajectories using the same ball. If we select the second trajectory to test this model against, with the following initial conditions

$$x = 0, \quad y = 0, \quad z = 0, \quad v_x = 68.221, \quad v_z = 12.701, \quad v_y = -4.961.$$

## 4.2 Parameterising $c_D$ and $c_L$ by Non Dimensional Variables

- We follow the idea from [Lieberman and Smits \(2001\)](#): form  $c_D$  and  $c_L$  from dimensionless groupings and use the data to estimate the parameters in this model.
- Use least squares to do this. See Appendix for discussion of what an inverse

problem is, how to use least squares to solve them, and what numerical techniques there are to do this.

- Find that doing this is very hard: the problem is likely not well posed and finding a minimum is difficult. Would benefit from a more through analysis of the least squares problem but unsure how this would be done.
- This inverse problem is a good way to move forwards with the problem in the future.

### 4.3 tanh Matching

- Take a hybrid approach between the two previous ideas: form a function which “looks” similar to [Morrison \(2010\)](#) and has the same behaviour, but is parameterised in such a way as to allow us to use a least squares solver to estimate parameters.
- For the drop, use a tanh function of the form

$$c_D = a + b \tanh(-c(Re - d))$$

where  $a, b, c, d$  are constants which we can use least squares to determine.

- Match the tanh at the top with the  $24/Re$  form we know from spheres and past the drop match to the weakly linear form we see from the previous work.
- Still trying to decide on results for this.

# Chapter 5

## Conclusions

### 5.1 Possible Future Work

# Appendix A

## Inverse Problems and Least Squares

### A.1 Inverse Problems

[Tarantola \(2005\)](#); [Tarantola and Valette \(1982\)](#)

### A.2 Least Squares

#### A.2.1 Guass-Newton Method

#### A.2.2 Levenberg-Marquardt Algorithm

[Pujol \(2007\)](#)

#### A.2.3 Trust Region Method

[Kelley \(1999\)](#)

### A.3 Well Posedness and Regularization

[Fang \(2004\)](#)

# Bibliography

- F. Alam, T. Steiner, H. Chowdhury, H. Moria, I. Khan, F. Aldawi, and A. Subic. A study of golf ball aerodynamic drag. *Procedia* ..., 13:226–231, 2011. doi: 10.1016/j.proeng.2011.05.077. URL <http://www.sciencedirect.com/science/article/pii/S187770581100991X>.
- J. D. Anderson. *Fundamentals of aerodynamics*. McGraw-Hill, 1985. ISBN 0071289089.
- K. Aoki, K. Muto, and H. Okanaga. Aerodynamic characteristics and flow pattern of a golf ball with rotation. *Procedia Engineering*, 2(2):2431–2436, June 2010. ISSN 18777058. doi: 10.1016/j.proeng.2010.04.011. URL <http://linkinghub.elsevier.com/retrieve/pii/S1877705810002651>.
- A. V. D. B. Assis, M. H. R. Tragtenberg, and N. S. Branco. Analytical calculation of the drag force near drag crisis of a falling sphere. (7):1–4, 9 2010. URL <http://arxiv.org/abs/1009.1536>.
- P. W. Bearman and J. K. Harvey. Golf ball aerodynamics. *The Aeronautical Quarterly*, 27:112–122, 1976. URL <http://scholar.google.com/scholar?hl=en&btnG=Search&q=intitle:Golf+ball+aerodynamics#0>.
- N. Beratlis, K. Squires, and E. Balaras. Numerical investigation of magnus effect on dimpled spheres. *Journal of Turbulence*, 13(June 2014):N15, 1 2012. ISSN 1468-5248. URL <http://www.tandfonline.com/doi/abs/10.1080/14685248.2012.676182>.
- J. M. Davies. The aerodynamics of golf balls. *Journal of Applied Physics*, 20(9): 821–828, 1949.

## Bibliography

- Q. Fang. Distinctions between LevenbergMarquardt method and Tikhonov regularization. *Dartmouth College Publication*, pages 1–7, 2004. URL [http://bbs.dartmouth.edu/~fangq/blog/doc/math/LM\\_Tik.pdf](http://bbs.dartmouth.edu/~fangq/blog/doc/math/LM_Tik.pdf).
- J. Jensen. Comment on 'the motion of an arbitrarily rotating spherical projectile and its application to ball games'. *Physica Scripta*, 89(6):067001, 6 2014. ISSN 0031-8949. URL <http://iopscience.iop.org/1402-4896/89/6/067001>.
- J. H. Jensen. Introducing fluid dynamics using dimensional analysis. *American Journal of Physics*, 81(9):688–694, 2013.
- C. T. Kelley. *Iterative methods for optimization*. SIAM, Philadelphia, 1999. ISBN 0898714338.
- J. R. Kensrud and L. V. Smith. In situ drag measurements of sports balls. *Procedia Engineering*, 2(2):2437–2442, June 2010. ISSN 18777058. doi: 10.1016/j.proeng.2010.04.012. URL <http://linkinghub.elsevier.com/retrieve/pii/S1877705810002663>.
- A. Kharlamov, Z. Chara, and P. Vlasak. Magnus and drag forces acting on golf ball. *Colloquium fluid dynamics, October*, (1959):1–9, 2007. URL <http://www.it.cas.cz/files/fluid-dynamics-2007/033-Kharlamov-PT.pdf>.
- T. Kray, J. Franke, and W. Frank. Magnus effect on a rotating sphere at high Reynolds numbers. *Journal of Wind Engineering and Industrial Aerodynamics*, 124:46–53, Nov. 2012. ISSN 01676105. doi: 10.1016/j.jweia.2013.10.010. URL <http://linkinghub.elsevier.com/retrieve/pii/S0167610512002097><http://linkinghub.elsevier.com/retrieve/pii/S0167610513002328>.
- J. Leong and C. Lin. Effects of golf ball dimple configuration on aerodynamics, trajectory, and acoustics. *Journal of flow visualization and image ...*, 2007. URL <http://www.dl.begellhouse.com/journals/52b74bd3689ab10b,622ede1536cd09e2,1d6f10f3366ac391.html>.
- B. Lieberman and A. Smits. Method for determining coefficients of lift and drag of a golf ball. *US Patent 6186002*, 2001. URL <http://www.google.com/patents/US6186002>.



- J. Martin, L. V. Smith, and J. R. Kensrud. Drag on sports balls using Doppler radar. *Procedia Engineering*, 34(1):134–139, Jan. 2012. ISSN 18777058. doi: 10.1016/j.proeng.2012.04.024. URL <http://linkinghub.elsevier.com/retrieve/pii/S1877705812016372>.
- T. Misic, M. Najdanovic-Lukic, and L. Nesic. Dimensional analysis in physics and the buckingham theorem. *European Journal of Physics*, 31(4):893, 2010. URL <http://stacks.iop.org/0143-0807/31/i=4/a=019>.
- F. Morrison. Data correlation for drag coefficient for sphere. *Michigan Technology University, Houghton, MI*, 6(April):1–2, 2010. URL <http://www.chem.mtu.edu/~fmorriso/DataCorrelationForSphereDrag2013.pdf>.
- T. Naruo and T. Mizota. The Influence of Golf Ball Dimples on Aerodynamic Characteristics. *Procedia Engineering*, 72:780–785, 2014. ISSN 18777058. doi: 10.1016/j.proeng.2014.06.132. URL <http://www.sciencedirect.com/science/article/pii/S1877705814006481>.
- A. R. Penner. The physics of golf. *Reports on Progress in Physics*, 66(2):131–171, 2003. URL <http://iopscience.iop.org/0034-4885/66/2/202/>.
- J. Pujol. The solution of nonlinear inverse problems and the Levenberg-Marquardt method. *Geophysics*, 72(4), 2007. URL <http://library.seg.org/doi/abs/10.1190/1.2732552>.
- G. Robinson and I. Robinson. The motion of an arbitrarily rotating spherical projectile and its application to ball games. *Physica Scripta*, 88(1):018101, July 2013. ISSN 0031-8949. doi: 10.1088/0031-8949/88/01/018101. URL <http://iopscience.iop.org/1402-4896/88/1/018101>.
- G. Robinson and I. Robinson. Reply to comment on 'the motion of an arbitrarily rotating spherical projectile and its application to ball games'. *Physica Scripta*, 89(6):067002, 6 2014. ISSN 0031-8949. URL <http://iopscience.iop.org/1402-4896/89/6/067002>.
- A. Ruban and J. Gajjar. *Fluid Dynamics I*. Oxford University Press, 1 edition, 2014. ISBN 978-0-19-968173-0.

## Bibliography

- W. R. Sears. *Introduction to Theoretical Aerodynamics and Hydrodynamics*. American Institute of Aeronautics and Astronautics, 2011. ISBN 1600867731.
- J. Seifert. A review of the Magnus effect in aeronautics. *Progress in Aerospace Sciences*, 55:17–45, Nov. 2012. ISSN 03760421. doi: 10.1016/j.paerosci.2012.07.001. URL <http://linkinghub.elsevier.com/retrieve/pii/S0376042112000656>.
- C. Smith, N. Beratlis, E. Balaras, K. Squires, and M. Tsunoda. Numerical investigation of the flow over a golf ball in the subcritical and supercritical regimes. *International Journal of Heat and Fluid Flow*, 31(3):262–273, June 2010. ISSN 0142727X. doi: 10.1016/j.ijheatfluidflow.2010.01.002. URL <http://linkinghub.elsevier.com/retrieve/pii/S0142727X10000147>.
- A. Smits and S. Ogg. Golf ball aerodynamics. *The Engineering of Sport*, 2004. URL <http://scholar.google.com/scholar?hl=en&btnG=Search&q=intitle:Golf+Ball+Aerodynamcs#2>.
- A. Tarantola. *Inverse problem theory and methods for model parameter estimation*. 2005. ISBN 0898715725. URL <http://epubs.siam.org/doi/book/10.1137/1.9780898717921>.
- A. Tarantola and B. Valette. Generalized nonlinear inverse problems solved using the least squares criterion. *Reviews of Geophysics*, 20(2):219–232, 1982. URL <http://onlinelibrary.wiley.com/doi/10.1029/RG020i002p00219/full>.
- H. Young and R. Freedman. *University Physics*. Addison Wesley, 12 edition, 2008. ISBN 0321501306.